

V. S. Morkun¹,
orcid.org/0000-0003-1506-9759,
N. V. Morkun¹,
orcid.org/0000-0002-1261-1170,
S. M. Hryshchenko^{*2},
orcid.org/0000-0003-4957-0904,
Y. O. Hryshchenko³,
orcid.org/0009-0002-0582-4140

1 – University of Bayreuth, Bayreuth, Federal Republic of Germany

2 – State Tax University, Irpin, Ukraine

3 – Volodymyr Dahl East Ukrainian National University, Kyiv, Ukraine

* Corresponding author e-mail: smgrischenko@gmail.com

INCREASING THE EFFICIENCY OF FINE WET GRINDING OF ORE USING THE DYNAMIC EFFECT OF ULTRASOUND

Purpose. The aim was to develop a method that would enhance the efficiency of classifying crushed ore by particle size, thereby preparing it for metallurgical process

Methodology. The following methods were used in the work: analysis of scientific and practical solutions; statistical methods for processing the results of experimental studies; methods of analytical synthesis; and methods of computer modeling for the synthesis and analysis of mathematical models.

Findings. The forces acting on crushed ore particles as they move in a layer of material on a vibrating screen have been investigated. The mechanism of contact interaction between solid-phase pulp particles has been substantiated, taking into account the geometry of contact surfaces, mechanical properties of materials, and loads applied to the contact. It has been proven that crushed ore particles and gas bubbles in the pulp flow, due to their individual characteristics (size, density, mass), each react in their own way to acoustic energy and the dynamic influence of ultrasonic vibrations applied and propagated in the medium. Based on the results of the analysis, it was concluded that ultrasound contributes to the diversity of dynamic reactions and increases the mobility of the components of the heterophasic structure of pulp materials. The conditions under which the influence of ultrasonic vibrations in ore pulp containing gas bubbles causes the destruction of ore aggregates and flocculates in it were analyzed. The parameters of ultrasonic vibrations that cause cavitation, the collapse of gas bubbles, and pressure surges of destructive amplitude in the pulp have been determined. It has been proven that acoustic emission arising from the propagation of ultrasonic vibrations in the pulp can be a general characteristic and property that determines the requirements for the form and parameters of controlling this process. A method for improving the efficiency of fine wet ore screening using the dynamic force of ultrasound on the classification product has been proposed.

Originality. A method has been developed to increase macrodiffusion and reduce the overall resistance to the movement of crushed ore pulp particles during screening by introducing ultrasonic vibrations of a certain amplitude and frequency into the oversize product of the screen, which allows increasing the speed of passage of crushed ore particles through the screen and reducing the proportion of unclassified product.

Practical value. The analysis of the results obtained shows an increase in the efficiency of fine wet screening of crushed ore by an average of 3 % due to ultrasonic treatment of the input product of the screen.

Keywords: *rumbling, vibration, classification, control, pulp, ultrasound, modelling*

Introduction. During the preparation of raw ore materials for metallurgical processing, involving many technological operations, the particle size of the crushed ore is gradually reduced. The purpose of these operations is to expose the grains of the useful component for its subsequent extraction into concentrate in enrichment devices. Currently, many mining and processing plants have begun to use fine wet screening screens to classify crushed ore by particle size. This approach has gained popularity because replacing the commonly used

mechanical spiral classifiers and hydrocyclones with them improves the quality of the final enrichment product, reduces the loss of useful components and processing costs, and increases productivity. In particular, reference [1] provides an example of installing a high-frequency screen after the fourth stage of magnetic separation with a screening size of 0.045 mm. Analysis of the results showed that this technological solution increases the iron content in the undersized product to 67.0 % compared to the existing content of 65 % in the concentrate of the existing plant. At the same time, it is noted that preliminary deflocculation of the input product is necessary to increase the efficiency of screening, release

non-metallic grains trapped in flocs, and improve the characteristics of the subsequent filtration process. Attention is also drawn to the rapid clogging of the sieving surface, which reduces the yield of fine grades in the undersized product and requires frequent stopping of the screens for cleaning or replacement of the sieves.

It is impossible to solve these problems by applying standard solutions in the conditions of modern intensive production [2]. Therefore, in order to transition to a new technological level and achieve high-quality indicators in mineral enrichment processes, the use of ultrasonic technologies is promising [3].

Literature review. Ore pulp is a heterogeneous medium consisting of crushed ore particles and gas bubbles. The concentration and fractional composition of both the solid and gas phases change as the raw materials and enrichment products move along the processing line. The effectiveness of using ultrasound in technological operations involving energy-intensive contact interaction primarily depends on understanding the behavior of solid-phase particles and gas bubbles in its force field.

The dynamic behavior of solid particles is based on interactions between them, such as contact forces and long-range non-contact forces (e.g., acoustic pressure force, Van der Waals force, capillary force, etc.) [2, 4]. Understanding these interactions is key to elucidating particle systems, as well as to designing and controlling the corresponding processes. The paper [4] reviews the achievements in the fundamental laws of particle interaction obtained using numerical methods in the range from the atomic to the continental scale. It also discusses the influence of friction and adhesion on particle packing, particle flow, mixing, destruction, and strengthening of particles in composites.

The study [5] determined the key parameters of physical properties, including apparent density, Young's modulus, and static and rolling friction coefficients, of iron ore pellets with different moisture contents. The measurement results showed that both the apparent density and Young's modulus of iron ore pellets generally decrease with moisture content due to the growth of the layer adhering to the particles. The coefficient of static friction generally increased with increasing moisture content, but at lower moisture contents, its fluctuations differed between granule types. The coefficient of rolling friction usually has a minimum value as the moisture content increases within the range considered.

In shear flows of concentrated suspensions, frequent collisions between particles significantly alter the dynamics and rheology of suspensions. Many of these changes cannot be attributed solely to viscous interactions; allowing contacts between solids during collisions, even when the suspended liquid is viscous and inertial effects are minimal, eliminates many qualitative discrepancies between models and experimental observations [6].

In [7], it was shown that the presence of solid particles in Newtonian fluid increases the effective viscosity of such a mixture. The increase depends on many factors, including the volume fraction of particles and their shape; spatial (e.g., gravitational) and surface (e.g., electrical) forces; and moments (e.g., magnetic) acting on the particles.

The paper [8] presents the main results of the study of bubble dynamics in a liquid, starting with Rayleigh's

model, which studied pressure prediction during the collapse of a spherical bubble, assuming that the surrounding liquid is incompressible. His work was expanded upon by Plesset, who derived a nonlinear second-order ordinary differential equation for the time-dependent evolution of the bubble radius. Improvements to this equation have been proposed by many authors, including Keller and Miksis [9], to include the effect of fluid compressibility on bubble dynamics and to study the propagation of waves emitted during collapse.

The characteristics of individual bubble oscillations, induced radiation pressure, and scattered power are important for a wide range of applications. For bubble oscillations with a high Mach number, the effect of fluid compressibility is significantly stronger and must be fully taken into account [10].

In study [11], the acceleration-induced expansion of a bubble and its non-spherical collapse in a rapidly changing pressure field under mechanical influence were modeled. Numerical results show that the cavitation bubble embryo rapidly expands in the pressure field caused by the impact, and the pressure wave is emitted and propagates in the liquid during the subsequent collapse of the bubble. When the pressure wave reflects off the wall, it causes a high-pressure peak on it, which can provoke the destruction of this obstacle.

When an acoustic wave interacts with a medium, two phenomena occur: forces caused by acoustic flow and forces caused by acoustic radiation. One of these phenomena, or a combination of both, manipulates the particles of the medium [12].

In [13], experiments and molecular dynamics modeling were used to lay the theoretical foundation for the industrial application of ultrasonic viscosity reduction, at least with regard to petroleum products. Viscosity was calculated using the Green–Kubo method, which is sufficient for low-pressure systems [14].

$$\eta = \frac{V}{3k_B T} \int_0^\infty dt \sum_\alpha \sum_\beta P_{\alpha\beta}(0) P_{\alpha\beta}(t),$$

where V is the volume of the system; k_B is Boltzmann's constant; T is the temperature of the system; α and β are directions in the Cartesian coordinate system; sharp brackets show the average value of the autocorrelation function in a balanced system; $P_{\alpha\beta}(t)$ is a component of the system shear stress in the α and β directions at time t .

It has been established that the total energy and temperature of the system increase rapidly after applying ultrasound to heavy oil macromolecules. The viscosity of heavy oil decreases significantly after ultrasound treatment, and this decrease in viscosity can reach 60 %. Ultrasound causes the macromolecules in heavy oil to break down into low-molecular-weight hydrocarbons, which causes the viscosity to decrease.

The paper [15] presents a mechanistic description of the energy conversion chain in an ultrasonic processor, which affects its energy efficiency. The gas content in the medium, both free and dissolved, affects several physical factors related to acoustics and cavitation phenomena. The underlying mechanism was elucidated through parallel analysis of experimental results and a mathematical model. A relationship between these factors was revealed. Finally, two examples are

presented, each relating to the physical process of ultrasonic cleaning and the chemical process of the Weissler reaction, which demonstrate the influence of gas content in the medium on the yield and efficiency of the process.

Ultrasonic treatment is an effective method for refining the dimensions and dispersing nanomaterials during their synthesis. In [16], it was found that the particle size decreased exponentially with increasing ultrasound power. A quantitative model was also proposed to describe the effect of ultrasound power on the size distribution of metal nanoparticles in terms of competition between surface energy and ultrasonic force.

Ultrasound remains an excellent method for forming emulsions for food products and other applications (e.g., cosmetics and pharmaceuticals) due to its high efficiency, excellent emulsion stability, and cost-effectiveness [17]. A problem is the low power of ultrasonic equipment and the undesirable distribution of acoustic waves through the medium during large-scale processing.

Purpose. The aim of the study is to develop a method for improving the efficiency of crushed ore classification based on particle size. The results of the research and examples of the application of ultrasonic methods indicate their potential for determining and forming the characteristics of liquid media containing solid-phase particles, gas bubbles, and their various aggregations and flocculation [2, 3]. At the same time, it should be noted that the mechanism of the effect of high-intensity ultrasound on such heterophasic structures and the interaction of its components in high-concentration suspensions requires further research. Another problem is the modeling of the specified contact interaction and movement of crushed ore particles with gas bubbles on the results of their passage through.

Methods. A trommel, as a classifying technological unit in the ore enrichment process, separates the incoming crushed product according to the size of its particles. This operation can be mathematically represented by the following operator [18]

$$\left\{ \begin{array}{l} \{Q_2^{(I)}, r_2^{(I)}[d], s_2^{(I)}[d]\}, \\ \{Q_2^{(II)}, r_2^{(II)}[d], s_2^{(II)}[d]\} \end{array} \right\} = \Lambda \left(\begin{array}{l} \{Q_1\}, \\ \{r_1[d], s_1[d]\}, t \end{array} \right),$$

where Λ is the noise operator; $\{Q_2^{(I)}, r_2^{(I)}[d], s_2^{(I)}[d]\}$ is the vector of output values of the subgrid product; $\{Q_2^{(II)}, r_2^{(II)}[d], s_2^{(II)}[d]\}$ is the vector of output values – supergrid product; $\{Q_1\}$ is the vector of control influences; $\{r_1[d], s_1[d]\}$ is the vector of disturbance influences (characteristics of the input flow of ore material).

A fully analytical representation of the screen operator Λ is impossible due to the complexity of the relationships between the output and input signals.

Among such signals in the rumbling process, the following elements of the operator should be highlighted:

- redistribution (change in particle size) of particles in the initial ore material flows

$$\begin{aligned} \{r_2^{(I)}[d]\} &= \Lambda(\{Q_1^{(II)}\}, \{r_1[d], s_1[d]\}, t); \\ \{r_2^{(II)}[d]\} &= \Lambda(\{Q_1^{(I)}\}, \{r_1[d], s_1[d]\}, t); \end{aligned}$$

- redistribution (due to changes in particle size) of iron content in the particle size classes of the initial ore material streams

$$\begin{aligned} \{s_2^{(I)}[d]\} &= \Lambda(\{Q_1^{(II)}\}, \{r_1[d], s_1[d]\}, t); \\ \{s_2^{(II)}[d]\} &= \Lambda(\{Q_1^{(I)}\}, \{r_1[d], s_1[d]\}, t). \end{aligned}$$

It should be noted that using the material balance equation, one of the screen outputs can be calculated based on the values of another output, for example, the output parameter $\{r_2^{(II)}[d]\}$ can be calculated based on the known output parameter $\{r_2^{(I)}[d]\}$ and input $\{r_1[d]\}$.

According to Newton's laws of motion, the translational and rotational motions of particle i and ore material during screening can be represented by the following expressions [19, 20]:

- for translational motion

$$m_i \frac{dv_i}{dt} = \sum_j (\mathbf{F}_{ij}^n + \mathbf{F}_{ij}^t) + \mathbf{F}_g;$$

- for rotary motion

$$I_i \frac{dw_i}{dt} = \sum_j \mathbf{T},$$

where m_i and I_i are the mass and moment of inertia of particle i , respectively; v_i and w_i are translational and angular velocities of the i^{th} particle, respectively; \mathbf{F}_g is gravitational force acting on a particle; \mathbf{F}_{ij}^n and \mathbf{F}_{ij}^t are normal and tangential contact forces, respectively; \mathbf{T} is torque acting on a particle, including rolling friction torque and tangential friction torque.

The Hertz-Mindlin contact model allows solving the above equations and finding the numerical values of the specified forces.

The normal force F_n can be determined by the normal overlap δ_n and is expressed as follows [20]

$$\mathbf{F}_n = \frac{4}{3} E^* \sqrt{R^*} \delta_n^{\frac{3}{2}}.$$

The equivalent Young's modulus E^* and equivalent radius R^* are defined as

$$\begin{aligned} E^* &= \frac{E_i E_j}{E_j(1-\nu_i^2) + E_i(1-\nu_j^2)}; \\ R^* &= \frac{R_j}{R_i + R_j}, \end{aligned}$$

where E_i , ν_i , R_i and E_j , ν_j , R_j are Young's modulus, Poisson's ratio, and the radius of each sphere in contact.

In addition, there is a damping force \mathbf{F}_n^d , which is defined as [20]

$$\mathbf{F}_n^d = -2\sqrt{\frac{5}{6}} \beta \sqrt{S_n m^*} v_n^{rel},$$

where $m^* = (m_i m_j)/(m_i + m_j)$ is equivalent mass; v_n^{rel} is normal component of relative velocity; S_n normal stiffness; β are defined as

$$\beta = -\frac{\ln e}{\sqrt{\ln^2 e + \pi^2}},$$

where e is the restitution coefficient.

The tangential force F_t depends on the tangential overlap δ_t and the tangential stiffness S_t [20, 21]

$$F_t = -S_t \delta_t,$$

where $S_t = 8G^* \sqrt{R^* \delta_n}$ is the equivalent shear modulus.

In addition, there is tangential damping, which is defined by [20, 21]

$$F_t^d = -2\sqrt{\frac{5}{6}} \beta \sqrt{S_t m^*} v_t^{rel},$$

where v_t^{rel} is the relative tangential velocity.

The tangential force is limited by Coulomb friction $\mu_s F_n$, where μ_s is the coefficient of static friction.

The main statistical parameters of a set of crushed ore particles describing the characteristics of contact forces and the force chain include the probability density distribution of the contact force and the average coordination number of particles [22].

The calculation of the probability density distribution relative to the normal contact force is as follows [23]

$$f_i^n = \frac{F_i^n}{\sum_{i=1}^N F_i^n / N},$$

where n is the normal contact force, i is the contact number; f_i^n is the standard value of normal contact force F_i^n ; F_i^n is the normalized value of the normal contact force of contact i ; N is the total number of such contacts.

Other forces of contact interaction can be normalized in a similar way.

The coordination number Z , also known as the average number of contacts, reflects the density of the contact network. The coordination number is defined as [22]

$$Z = \frac{2N_c}{N_p},$$

where N_c is the number of contacts in the particle aggregate (contacts with normal contact force greater than 0); N_p is the number of particles.

The coordination number can be understood as the average number of particles in contact with each particle, which to a certain extent reflects the state of the granular material in the measured area (in terms of factors such as stress level and contact force distribution intensity).

In an ultrasonic field, solid particles, gas bubbles, and their aggregates suspended in an acoustically controlled liquid are subjected to constant (time-averaged) hydrodynamic forces that cause them to move, group together in certain areas of space, interact with each other, etc. [2, 24]. With respect to any body immersed in a liquid, these forces are defined as acoustic radiation pressure forces and can be represented in tensor form as [24]

$$F_i = \int_S \sigma_{ik} n_k dS,$$

where S is the surface of the body, n_k is the unit external normal to S ; σ_{ik} is the stress tensor in the fluid

$$\sigma_{ik} = -p \delta_{ik},$$

where p is the fluid pressure; δ_{ik} is the Kronecker delta.

The acoustic radiation forces acting on gas bubbles (Bjerknes forces) are divided into two types, namely primary Bjerknes forces, which act on individual bubbles, and secondary Bjerknes forces, which are responsible for the interaction between bubbles. Primary forces cause bubbles to migrate in the acoustic field or gather in certain areas, such as pressure nodes or antinodes of standing sound waves. Secondary forces cause them to attract or repel each other and can also lead to stable bubbles under certain conditions. Mathematically, the Bjerknes force is calculated as the time average of a certain expression, which is the instantaneous force acting on a bubble by the surrounding (acoustically excited) fluid [25].

Results. To determine the parameters of elastic contact between crushed ore particles when they collide during movement in the screening process, the HertzWin calculator [26] was used, which implements the basic properties of the Hertz-Mindlin contact model [19–21].

Elastic energy is the integral of the force $F(dZ)$. This energy contributes to the formation of stresses and strains in the particles, as well as the speed and trajectory of their further motion.

For circular contact, the elastic energy E_j is equal to [26]

$$E_j = \int F(E, R, \delta Z) d\delta Z = \int \frac{4E\sqrt{R}\delta Z^{\frac{3}{2}}}{3} d\delta Z,$$

where R is the contact radius; δZ is the total compression.

Contact force causes deformation and, consequently, stress in the material particles. Stress in point contacts is distributed unevenly. Most stresses in the general contact zone slowly decrease with increasing distance from the contact. However, the shear stress reaches its maximum at some distance from the contact surface.

Compression of bodies during force contact occurs nonlinearly, with contact stiffness depending on the applied force. For spherical contact, compression δZ is determined by the expression [26]

$$\delta Z = \left(\frac{9F^2}{16RE^2} \right)^{\frac{1}{3}}.$$

Therefore, the contact force divided by the total compression is equal to

$$\frac{F}{\delta Z} = \left(\frac{16RE^2 F}{9} \right)^{\frac{1}{3}}.$$

Local stiffness C_z is derived from compression [26]

$$C_z = \frac{3}{2} \left(\frac{16RE^2 F}{9} \right)^{\frac{1}{3}} = \frac{3}{2} \frac{F}{\delta Z}.$$

Below are graphs of stresses in elliptical ore particles during elastic collision. The dependencies shown are calculated for contact conditions, the parameters of which are given in Table.

Table uses the following symbols: p_1 is density, g/cm^3 ; p_2 is Young's modulus, GPa; p_3 is shear modulus, kg/mm^2 ; p_4 is Poisson's ratio; p_5 is dimensions $r_{1a} \cdot r_{1b}$, mm; p_6 is dimensions $r_{2a} \cdot r_{2b}$, mm; p_7 is the contact angle, degrees; p_8 is external force, H.

Table

Parameters of ore particle contact

p_1	p_2	p_3	p_4	p_5	p_6	p_7	p_8
2.520	68.33	27.06	0.258	0.15 · 0.1	0.074 · 0.12	30	6

Fig. 1 shows graphs of subsurface stresses in an ore particle during force contact interaction along the Z axis.

The subsurface stress dependencies shown in Fig. 1 belong to the contact center. The horizontal axis shows stress in MPa. Contact occurs between elliptical parts, the dimensions of which are determined by the radii along its two axes r_{1a} and r_{1b} .

Thus, the geometry of contact surfaces, the mechanical properties of materials, and the loads applied to the contact determine the mechanism of interaction between crushed ore particles when they collide. These factors form the stress at the point of contact and the trajectory of particle movement in the environment in which they are located.

When ultrasonic waves propagate in the pulp, their energy is absorbed and scattered by ore particles and gas bubbles. To characterize the absorption and scattering of acoustic vibrations by these inclusions in the pulp, the concepts of effective cross sections of extinction σ_p , absorption σ_c and scattering σ_s are introduced. Under effective cross-sectional repayment (attenuation) σ_p , this refers to the cross-sectional area perpendicular to the direction of the sound wave, for which the incoming acoustic energy is equal to the sum of the energy absorbed and scattered by inclusions, i.e. [27]

$$\sigma_p = \sigma_c + \sigma_s,$$

The absorption cross section σ_{sc} determines the proportion of energy absorbed by the solid phase particle. These energy losses are caused by friction (viscosity) during particle vibrations. For a spherical particle with radius r and density ρ_1 the absorption cross section is determined by the formula [27]

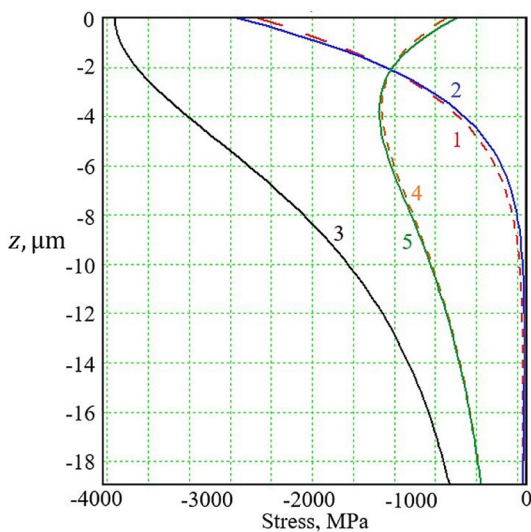


Fig. 1. Subsurface stresses:

1 – $Sa(Z)$; 2 – $Sb(Z)$; 3 – $Sz(Z)$ – compressive stresses in the particle in the corresponding directions; 4, 5 – shear stresses $Ta(Z)$, $Tb(Z)$ in the particle, the size of which is given $r_{1a} \cdot r_{1b}$

$$\sigma_{sc}(\lambda) = \frac{4\pi r^3}{3} k \left(\frac{\rho_1}{\rho_0} - 1 \right)^2 \frac{S}{S^2 + (\rho_1/\rho_0 + \tau)^2},$$

where $k = 2\pi/\lambda$ is the wave number; ρ_0 is the density of the fluid;

$$S = \frac{9}{4Br} \left(1 + \frac{1}{Br} \right); \quad B = (\pi v/\mu)^{\frac{1}{2}};$$

$$\tau = \frac{1}{2} + \frac{9}{4Br}; \quad \mu = \eta/\rho_0,$$

where η is the fluid viscosity coefficient; v is ultrasonic vibration frequency.

Diffraction phenomena caused by media inhomogeneities lead to the scattering of sound wave energy. The cross-section of this process is determined by the expression [27]

$$\sigma_{ss}(\lambda) = \frac{4\pi r^3}{3} \cdot \frac{1}{6} k^4 \cdot r^3,$$

where k is the wave number; r is the particle radius.

The presence of gas bubbles in the pulp also leads to the absorption and scattering of acoustic energy.

Unlike solid phase particles, absorption and scattering on gas bubbles is resonant in nature. Absorption cross sections $\sigma_{gc}(\lambda)$ and scattering $\sigma_{gs}(\lambda)$ gas bubbles are determined by the formulas [27]

$$\sigma_{gc}(\lambda) = \frac{4\pi R^2 (\delta/k_1 - 1)}{(v_0^2/v^2 - 1)^2 + \delta^2};$$

$$\sigma_{gs}(\lambda) = \frac{4\pi R^2 (\delta/k_1)}{(v_0^2/v^2 - 1)^2 + \delta^2},$$

where v_0 is the resonance frequency of a bubble with radius R ; δ is the decay constant; $k_1 = 2\pi R/\lambda$.

The expressions show that the maximum cross-sectional values are achieved at $v = v_0$.

The total cross section for the absorption of acoustic energy by a gas bubble is determined by the sum of $\sigma_{gc}(\lambda)$ and $\sigma_{gs}(\lambda)$

$$\sigma_{gp} = \sigma_{gc}(\lambda) + \sigma_{gs}(\lambda) = \frac{4\pi R^2}{(v_0^2/v^2 - 1)^2 + \delta^2}.$$

From the above, it can be concluded that each particle of the crushed ore and each gas bubble, due to its individual characteristics (size, density, mass), reacts differently to the acoustic energy and dynamic impact of ultrasonic vibrations applied and propagated in the pulp. That is, ultrasound promotes a variety of dynamic reactions and increases the mobility of its heterophase structure components.

An important element of the process of ultrasound propagation in a liquid containing gas bubbles is the phenomena accompanying their cavitation collapse. To model the dynamics and acoustic radiation of a cavitation bubble, the Keller-Miksis equations [9] and the methods given in [11] were used. The dynamics of a gas bubble is determined by the expression

$$\left(1 - \frac{\dot{R}}{c} \right) R \ddot{R} + \left(\frac{3}{2} - \frac{\dot{R}}{2c} \right) \dot{R}^2 = \frac{1}{\rho} \left(1 + \frac{\dot{R}}{c} \right) p_w + \frac{R}{\rho c} \frac{dp_w}{dt},$$

where R is the instantaneous radius of the bubble as a function of time; t is time; c is the speed of sound in the

medium; ρ is the density of water; p_w is the pressure on the bubble wall.

The pressure on the bubble wall in the zone of ultrasonic impact is calculated

$$p_w = \left(P_0 + \frac{2\sigma}{R_0} \right) \left(\frac{R_0}{R} \right)^{3k} - \frac{2\sigma}{R} - \frac{4\eta\dot{R}}{R} - P_0 - P_a \sin(\omega t),$$

where σ is the surface tension at the gas-water interface; η is the dynamic viscosity of water; R_0 is the equilibrium radius of the bubble; k is the polytropy index; P_a is the amplitude of ultrasonic pressure.

The amplitude of acoustic emission of a cavitation bubble is inversely proportional to the distance from its center

$$P_{rad} = \rho \frac{\ddot{R}R^2 + 2R\dot{R}^2}{r},$$

where P_{rad} is the acoustic emission; r is the distance from the center of the bubble to the observation point.

Fig. 2 shows the dynamics of a bubble with a radius $R_0 = 50 \mu\text{m}$ in an ultrasound field of 21.5 kHz.

The cavitation collapse of a gas bubble is accompanied by changes in pressure, as shown in the dependence shown in Fig. 3.

That is, ultrasonic vibrations in a liquid containing gas bubbles, under certain conditions, cause pressure surges of destructive amplitude in the space close to it.

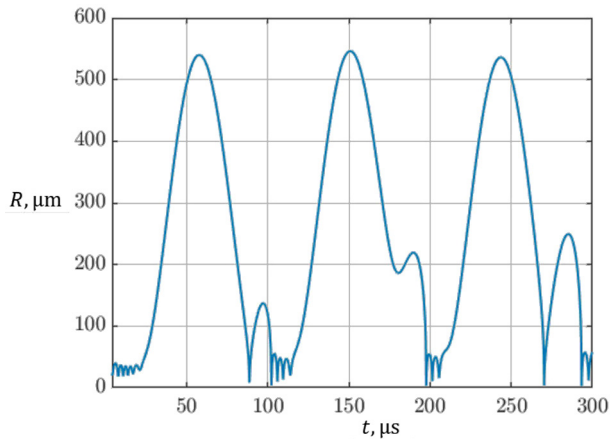


Fig. 2. Changes in the size of a gas bubble (primary radius $50 \mu\text{m}$) under the influence of ultrasonic waves with a frequency of 21.5 kHz

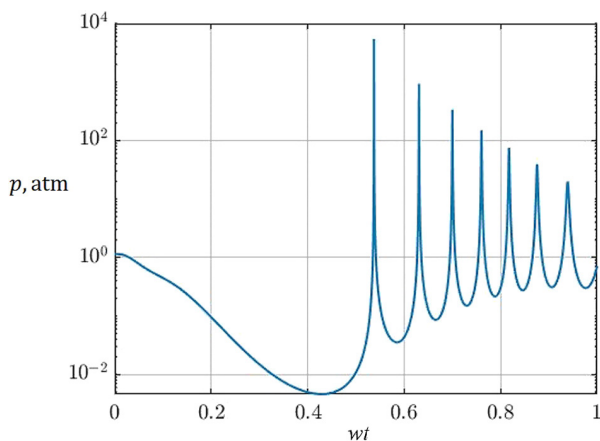


Fig. 3. Pressure changes during cavitation collapse of a gas bubble

Thus, the reaction shown in Fig. 3 contributes to the destruction of ore aggregations and flocculoformations in the pulp. It should also be noted that there are numerous harmonic components of the pressure (Fig. 4) emitted by the cavitation bubble, which is a consequence of the fact that cavitation is inherently a nonlinear response to ultrasonic irradiation of the medium under study

The processes occurring in the ore material moving along the sieve under the influence of the above forces are modeled in a program that implements numerical analysis and graphical representation of the results of changes in the granulometric characteristics of the solid phase of the pulp in the over-grid product of the screen. The geometry of measurements, the position of the source and the intensity of ultrasonic vibrations, and the concentration of solid-phase particles, and their size distribution are set before the start of the simulation. The measurement area is represented by a sieve model, the length and inclination of which can be changed depending on the task at hand. The measurement range is set by sections along the length of the sieve, in which the number of particles that fall into them is counted. The ordinate axis (Fig. 5) shows the number of processed particles, with the scale automatically expanding as the simulation time increases, i.e., the number of particles, and the abscissa axis shows the distance, cm.

Fig. 5 shows the results of modeling the movement of crushed ore particles in the screen over-mesh product, which are transmitted by the vibrations of the sieve surface.

The granulometric characteristic of the product is given by 5 size classes from 44 to 150 microns. The density of the crushed ore particles in the model example is $2.0\text{--}4.2 \text{ g/cm}^3$. The primary concentration of the pulp solid phase is 1.65 g/cm^3 .

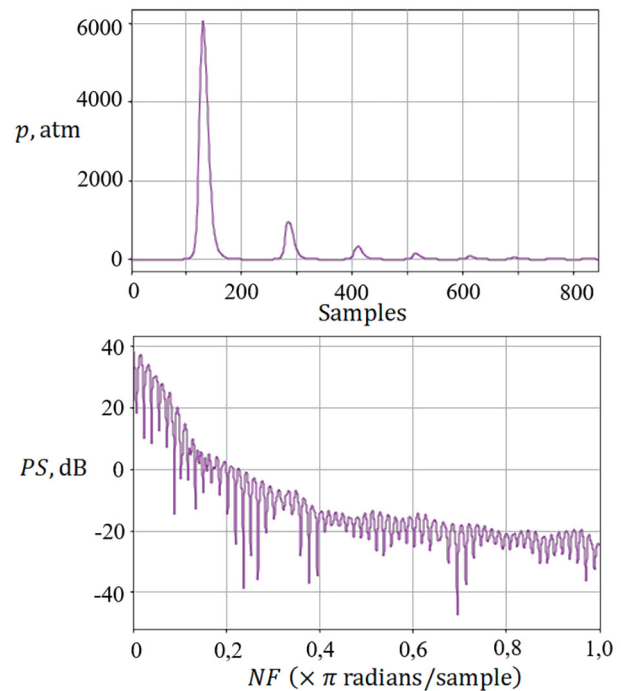


Fig. 4. Spectral analysis of cavitation bubble radiation: PS – spectral power of pressure p ; NF – normalized frequency

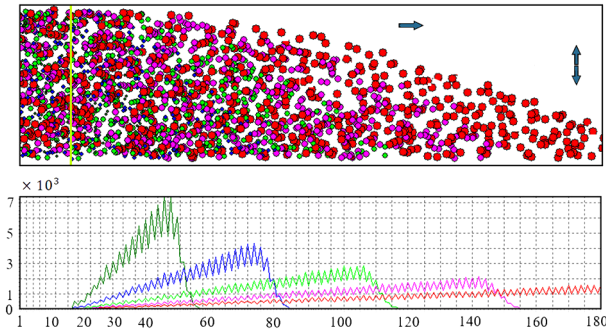


Fig. 5. The results of modeling the movement of crushed ore particles in the over-grid product of the screen

The simulation results demonstrate the independence of the particle size distribution law from the number of particles and the simulation time.

That is, in contrast to the existing assumption of perfect mixing of ore particles in the layer above the sieve, the modeling results indicate that large grains prevail in the upper part of the layer and small ones in the lower part. The above mechanism of ultrasound propagation in the pulp contributes to an increase in the macrodiffusion coefficient and a decrease in the resistance of the medium itself and the braking force of a set of particles when one of them moves through their layer. This increases the overall speed of particle passage of the crushed ore through the screen sieve.

In order to experimentally verify the effect of ultrasound on the process of fine wet screening of ore, a setup that is a scaled model of an industrial screen was used. Ultrasonic vibrations were introduced directly into the inlet stream of the screen. Product characteristics were determined, and the screening efficiency was quantified using standard laboratory methods. The acoustic and energy characteristics of the ultrasonic impact system (UIS) used in the study are shown in Fig. 6. The source of electric ultrasonic vibrations is an ultrasonic generator with acoustic feedback and a maximum output power of 300 W. The operating resonant frequency of the ultrasonic impact system is 21.5 kHz.

The effect of ultrasonic irradiation of the pulp on the efficiency of screening under different modes of operation of the screen (amplitude, vibration frequency, surface angle, and quantitative and qualitative characteristics of the pulp flow) was studied.

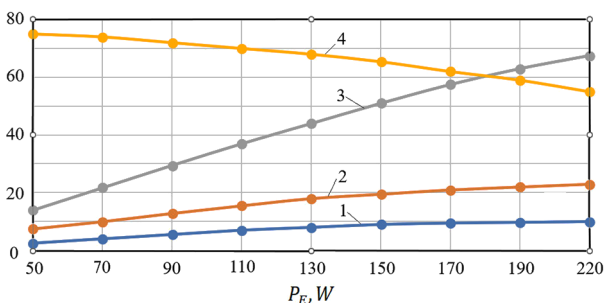


Fig. 6. Acoustic and energy characteristics of the ultrasonic impact system:

P_E, Bm – electric power consumption; 1 – volumetric density of acoustic energy, $EVA/20, J/cm^3$; 2 – acoustic power released in the load, $P_A \cdot 5, W$ is the amplitude of the waveguide end, $A/2, \mu m$; 4 – is the efficiency of the SWS, $\eta, \%$

The efficiency of the screening process was determined by the following expression [28].

$$\eta = \frac{m_{Sp}}{m_{St}} \cdot 100 \%,$$

where m_{Sp} is the total mass of sifted particles in the collection box under the sieve plate, the size of which is smaller than the sieve opening; m_{St} is the total mass of particles in the input product, the size of which is smaller than the sieve aperture.

Fig. 7 shows the results of the effect of ultrasound on the dependence of screening efficiency on the amplitude of screen vibration.

The dependencies shown in Fig. 7 are approximated by the following polynomial equations

$$y_1 = 0.055x^3 - 1,528x^2 + 11,417 + 69,617;$$

$$R^2 = 0.986;$$

$$y_2 = 0.041x^3 - 1,451x^2 + 12,304 + 62,415;$$

$$R^2 = 0.994.$$

The analysis of the obtained results shows a decrease in the proportion of unclassified particles (particles whose size is smaller than the sieve opening but falling into the under-sieve product), i.e., an increase in the efficiency of fine wet screening of crushed ore by an average of up to 3 % due to the ultrasonic treatment of the screen input product.

Conclusions. When a particle of crushed ore moves in a layer of material on a screen, it is affected by the resistance force of the medium (viscosity) and the resistance force of the surrounding particles as the particle tries to pass through them. The geometry of the contact surfaces, the mechanical properties of the materials, and the loads applied to the contact determine the mechanism of interaction between the crushed ore particles when they collide. These factors form the stresses in the point contact and the trajectories of the particles in the environment in which they are located.

Due to their individual characteristics (size, density, mass), the particles of the crushed ore and gas bubbles in the pulp flow each react differently to the acoustic energy and dynamic impact of ultrasonic vibrations applied and propagated in the medium. That is, ultrasound contributes to the diversity of the dynamic response and increases the mobility of the components of its heterophase structure.

Ultrasonic vibrations in a liquid containing gas bubbles, under certain conditions, cause pressure surges of

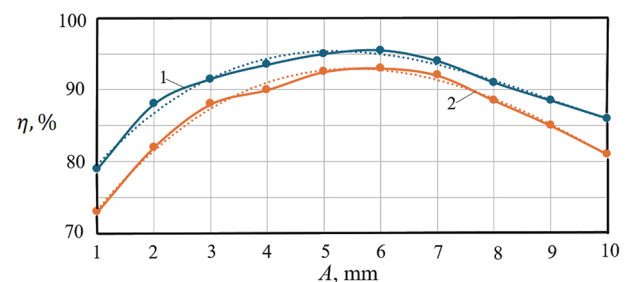


Fig. 7. Results of ultrasound impact on the dependence of screening efficiency on the screen vibration amplitude:

1 – with ultrasonic impact; 2 – without ultrasonic impact

destructive amplitude in the space close to them. This reaction contributes to the elimination of ore aggregations and flocculoformations in the pulp.

The acoustic emission formed under the influence of ultrasonic irradiation of the pulp caused by the cavitation collapse of gas bubbles is a manifestation of a complex nonlinear process that includes numerous harmonic components. This can be a general characteristic and property that determines the requirements for the shape and control parameters of this process.

The considered mechanism of ultrasound propagation in the pulp contributes to an increase in the macro-diffusion coefficient, a decrease in the total coefficient of resistance of the medium, an increase in the speed of passage of particles by the crushed ore through the screen, and a decrease in the proportion of unclassified product. The efficiency of ore screening increases by an average of 3 %.

References.

1. Oliinyk, T. A., Sklyar, L. V., Oliinyk, M. O., Kushniruk, N. V., Sklyar, A. Yu., & Korzhan, I. A. (2018). Use of fine screening at PJSC Northern GOK. *Enrichment of minerals*, 69(110), 69-77.
2. Morkun, V., & Morkun, N. (2018). Estimation of the crushed ore particles density in the pulp flow based on the dynamic effects of high-energy ultrasound. *Archives of Acoustics*, 43(1), 61-67. <https://doi.org/10.24425/118080>
3. Morkun, V., Pikilnyak, A., & Morkun, N. (2014). Simulation of the Lamb waves propagation on the plate which contacts with gas containing iron ore pulp in Waveform Revealer toolbox. *Metallurgical and Mining Industry*, 6(5), 16-19.
4. Zheng, Q., Yang, R., Zeng, Q., Zhu, H., Dong, K., & Yu, A. (2024). Interparticle forces and their effects in particulate systems. *Powder Technology*, 436, 119445. <https://doi.org/10.1016/j.powtec.2024.119445>
5. Li, C., Moreno-Atanasio R., O'dea, D., & Honeyands, T. (2019). Experimental Study on the Physical Properties of Iron Ore Granules Made from Australian Iron Ores. *ISIJ International*, 59(2), 253-262. <https://doi.org/10.2355/isijinternational.ISIJINT-2018-508>
6. Zhang, H., Kopelevich, D.I., & Butler, J. (2024). Frictional effects on shear-induced diffusion in suspensions of non-Brownian particles. *Journal of Fluid Mechanics*, 1001(A42). <https://doi.org/10.1017/jfm.2024.1121>
7. Abedian, B., & Kachanov, M. (2010). On the effective viscosity of suspensions. *International Journal of Engineering Science*, 48(11), 962-965. <https://doi.org/10.1016/j.ijengsci.2010.08.012>
8. Fourest, T., Deletomb, É., Faucher, V., Arrigoni, M., Dupas, J., & Laurens, J.-M. (2018). Comparison of Keller-Miksis model and finite element bubble dynamics simulations in a confined medium. Application to the hydrodynamic ram. *European Journal of Mechanics B/Fluids*, 68, 66-75. <https://doi.org/10.1016/j.euromechflu.2017.11.004>
9. Bao, H., Reuter, F., Zhang, H., & Lu, J. (2023). Impact-driven cavitation bubble dynamics. *Experiments in Fluids*, 64(27). <https://doi.org/10.1007/s00348-023-03569-z>
10. Zheng, X., Wang, X., Zhang, Y., & Zhang, Y. (2022). A single oscillating bubble in liquids with high Mach number. *Ultrasonics Sonochemistry*, 85, 105985. <https://doi.org/10.1016/j.ultsonch.2022.105985>
11. Chen, Y. han, Zhan, J. Min, & Li, Y. tian (2021). Numerical simulation of cavitation-bubble expansion and collapse inside a bottle subjected to impact on its topside. *Engineering Applications of Computational Fluid Mechanics*, 5(1), 1440-1451. <https://doi.org/10.1080/19942060.2021.1976279>
12. Wang, S., Wang, X., You, F., & Xiao, H. (2023). Review of Ultrasonic Particle Manipulation Techniques: Applications and Research Advances. *Micromachines*, 14(8), 1487. <https://doi.org/10.3390/mi14081487>
13. Shi, J., Tong, L., Sun, L., Jiang, T., Yu, X., Yu, K., Lu, S., & Xu, W. (2024). Molecular Dynamics Simulation on the Process of Ultrasonic Viscosity Reduction. *Processes*, 12(12), 2803. <https://doi.org/10.3390/pr12122803>
14. Zhang, Z., Zhang, W., Zhang, J., Sun, H., & Li, X. (2011). Simulations of physical properties of air by molecular dynamics method introduced the rotations of diatomic molecules and the momentum control. *Journal of Molecular Science*, 27, 203-207. <https://doi.org/10.13563/j.cnki.jmolsci.2011.03.012>

15. Suryakant, V. Moholkar, Sivasankar, T., Bhaskar, J. C., & Roy, K. (2022). Energy Aspects of Acoustic Cavitation and Sonochemistry/Chapter 12 – Mechanistic issues of energy efficiency of an ultrasonic process: Role of free and dissolved gas. *Fundamentals and Engineering*, 193-219. <https://doi.org/10.1016/B978-0-323-91937-1.00002-5>
16. Yang, G., Lin, W., Lai, H., Tong, J., Lei, J., Yuan, M., Zhang, Yu., & Cui, C. (2021). Understanding the relationship between particle size and ultrasonic treatment during the synthesis of metal nanoparticles. *Ultrasonics Sonochemistry*, 73, 105497. <https://doi.org/10.1016/j.ultsonch.2021.105497>
17. Tiang, S. S. L., Low, L.E., Ali, I., Zhou, L., Goh, B.-H., Gew, L. T., & Tang, S.Y. (2024). Recent advances in ultrasonic cavitation technologies for emulsion preparation: a mini review. *Current Opinion in Chemical Engineering*, 45, 101046. <https://doi.org/10.1016/j.coche.2024.101046>
18. Morkun, V., Tron, V., & Zymohliad, V. (2022). Modelling of Iron Ore Processing in Technological Units Based on the Hybrid Approach. *Acta Mechanica et Automatica*, 16(1), 82-90. <https://doi.org/10.2478/ama-2022-0010>
19. Xu, N., Tang, S., Lin, D., Geng, R., Wang, X., & Liang, X. (2024). Complex granular flows of sticky-wet material on flip-flow screens: Calibration of discrete element simulations. *Particuology*, 84, 290-308. <https://doi.org/10.1016/j.partic.2023.07.010>
20. Dai, S., Zhang, S., Gao, F., He, X., & Sheng, D. (2024). Investigation of particle segregation in a vertically vibrated binary mixture: Segregation process and mechanism. *Computers and Geotechnics*, 169, 106236. <https://doi.org/10.1016/j.compgeo.2024.106236>
21. Pan, W., Hou, X., Ding, T., & Tang, D. (2015). Tangential force model study of lunar dust particles based on Hertz-Mindlin theory and sensor technology. *Sensor Letters*, 13, 176-179. <https://doi.org/10.1166/sl.2015.3463>
22. Chen, Q., Qin, S., & Wu, S. (2020). Quantitative Study on the Contact Force and Force Chain Characteristics of Ore Particle Systems during Ore Drawing from a Single Drawpoint under the Influence of a Flexible Barrier. *Geofluids*, 127076, 13. <https://doi.org/10.1155/2020/1270761>
23. Zhang, W., Zhou, J., Yu, S. W., Zhang, X. J., & Liu, K. (2018). Investigation on contact force and force chain of granular matter in biaxial compression. *Chinese Journal of Applied Mechanics*, 35, 530-538.
24. Chassaing, P. (2022). *Fundamentals of Fluid Mechanics* (ed. 1), XXI. ISBN 978-3-031-10086-4.
25. Zhang, X., Li, F., Wang, C., Mo, R., Hu, J., Guo, J., & Lin, S. (2022). Effects of translational motion on the Bjerknes forces of bubbles activated by strong acoustic waves. *Ultrasonics*, 126, 106809. <https://doi.org/10.1016/j.ultras.2022.106809>
26. Hertz Contact Stress Calculations. Retrieved from <https://vinksda.com/toolkit-mechanical-calculations/hertz-contact-stress-calculations/>
27. Morkun, V., Morkun, N., Tron, V., & Hryshchenko, S. (2017). Investigation of the effect of characteristics of gas-containing suspensions on the parameters of the process of ultrasonic wave propagation. *Eastern-European Journal of Enterprise Technologies*, 6.5(90), 49-58. <https://doi.org/10.15587/1729-4061.2017.118943>
28. Chen, B., Yan, J., Mo, W., Xu, W., Zhang, L., & Tamma Kumar, K. (2019). DEM simulation and experimental study on the screening process of elliptical vibration mechanical systems. *Journal of vibroengineering*, 21(8). <https://doi.org/10.21595/jve.2019.19993>

Підвищення ефективності тонкого вологого грохочення руди із застосуванням динамічного впливу ультразвуку

В. С. Моркун¹, Н. В. Моркун¹, С. М. Грищенко^{*2}, Я. О. Грищенко³

1 – Байройтський університет, м. Байройт, Федеративна Республіка Німеччина

2 – Державний податковий університет, м. Ірпінь, Україна

3 – Східноукраїнський національний університет імені Володимира Даля, м. Київ, Україна

* Автор-кореспондент e-mail: smgrischenko@gmail.com

Мета. Розробка методу підвищення ефективності класифікації подрібненої руди за крупністю її

часток у процесі підготовки до металургійного перелілу.

Методика. У роботі використані такі методи: аналіз наукових і практичних рішень; статистичні методи для оброблення результатів експериментальних досліджень; методи аналітичного синтезу; методи комп'ютерного моделювання для синтезу й аналізу математичних моделей.

Результати. Досліджені сили, що діють на частинки подрібненої руди при їх русі у шарі матеріалу на ситі грохота. Обґрунтовано механізм контактної взаємодії частинок твердої фази пульпи з урахуванням геометрії контактних поверхонь, механічних властивостей матеріалів і навантажень, що прикладаються до контакту. Доведено, що частинки подрібненої руди й газові бульбашки в потоці пульпи, у силу своїх індивідуальних характеристичних ознак (крупність, щільність, маса), кожна по своєму реагують на акустичну енергію та динамічний вплив ультразвукових коливань, що прикладені й розповсюджуються у середовищі. За результатами виконаного аналізу зроблено висновок, що ультразвук сприяє різноманітності динамічної реакції та підвищенню рухомості складових гетерофазної структури пульпових матеріалів. Проаналізовані умови, за яких вплив ультразвукових коливань у рудній пульпі, що включає газові бульбашки, викликає руйнацію в ній рудних агрегацій і флокулоутворень. Визначені параметри ультразвукових

коливань, що викликають кавітаційний колапс газових бульбашок і сплески тиску руйнівної амплітуди у пульпі. Доведено, що акустична емісія, що виникає при розповсюдженні ультразвукових коливань у пульпі, може бути загальною характеристикою та властивістю, що обумовлюють вимоги до форми й параметрів керування цим процесом. Запропоновано метод підвищення ефективності тонкого вологого грохочення руди із застосуванням динамічного силового впливу ультразвуку на продукт класифікації.

Наукова новизна. Розроблено метод підвищення макродифузії та зменшення загального опору руху подрібнених частинок рудної пульпи у процесі її грохочення шляхом уведення у надрешітний продукт грохота ультразвукових коливань певної амплітуди й частоти, що дозволяє збільшити швидкість проходження частинок подрібненої руди через сито грохота та зменшити частку некласифікованого продукту.

Практична значимість. Аналіз отриманих результатів свідчить про підвищення ефективності тонкого вологого грохочення подрібненої руди в середньому до 3 % за рахунок ультразвукового оброблення вхідного продукту грохота.

Ключові слова: грохот, вібрація, класифікація, керування, пульпа, ультразвук, моделювання

The manuscript was submitted 27.03.25.